Journal of the Serbian Chemical Society
JSCS-info@shd.org.rs • www.shd.org.rs/JSCS

ACCEPTED MANUSCRIPT

Journal of the Serbian Chemical Society
JSCS-info@shd.org.rs • www.shd.org.rs/JSCS
J. Serb. Chem. Soc. **00(0)** 1-16 (2026)
JSCS–13418
Original scientific paper
Published DD MM, 2026

Fabrication of visible-light photoactive $TiO_2/BiVO_4$ composite for photocatalytic degradation of ciprofloxacin

THU LOAN DANG[1], VU VAN TU[2], THI HUE NGUYEN[2], DUC VAN NGUYEN[3]*, AND THI THAO TA[1§]

[1]Faculty of Chemistry, VNU University of Science, 19 Le Thanh Tong, 100000, Vietnam, [2]Institute of Science and Technology for Energy and Environment, Vietnam Academy of Science and Technology, 18 Hoang Quoc Viet, Nghia Do Ward, Hanoi 100000, Vietnam, and [3]Institute of Materials Science, Vietnam Academy of Science and Technology, 18 Hoang Quoc Viet, Nghia Do Ward, Hanoi 100000, Vietnam.

(Received 13 June; revised 30 June; accepted 2 December 2025)

Abstract: Pure $BiVO_4$ and three $TiO_2/BiVO_4$ composite photocatalysts with Bi^{3+}:Ti^{4+} molar ratios of 1:1, 2:1, and 4:1 were readily synthesized for the first time using a one-pot hydrothermal procedure for the photodegradation of ciprofloxacin. Conducting the hydrothermal reaction in a basic medium yielded single-phase scheelite monoclinic polymorphic $BiVO_4$ (*ms*-$BiVO_4$) in the composite samples. Microstructural analysis showed spherical TiO_2 nanoparticles with an average grain size of 120 nm embedded on the surface of $BiVO_4$ nanoplates. The optimized composite exhibited a ciprofloxacin photodegradation reaction rate constant was about 3.8 times higher than that of the pure $BiVO_4$ sample. This significant enhancement is attributed to the formation of a $TiO_2/BiVO_4$ heterojunction, which promotes efficient charge separation. This research expands the knowledge on designing of $BiVO_4$-rich composites (with Bi^{3+}:Ti^{4+} molar ratio ≥ 1:1) via heterogeneous junction engineering to enhance photocatalytic activity beyond that of pure $BiVO_4$. This research also provided a perspective on using the $BiVO_4$-rich composites as effective photocatalysts as degradation of antibiotics in aqueous media under visible-light irradiation.

Keywords: photocatalysis; semiconductor; heterojunctions; antibiotic residues; hydrothermal.

INTRODUCTION

Over the last years, the widespread use of antibiotics in veterinary and human medicine has resulted in an increased potential for water contamination, even at trace concentrations.[1–2] Particularly, it is estimated that many tons of antibiotic

* Corresponding author. E-mail: vannd@ims.vast.ac.vn; § tathithao@hus.edu.vn
https://doi.org/10.2298/JSC250613001D

residues are released into the environment in Southeast Asia annually.[3] The World Health Organization (WHO) typically reports that pharmaceutical concentrations in surface waters, groundwater, and partially treated water were below 0.1 μg L^{-1} (or 100 ng L^{-1}), and concentrations in treated water were generally below 0.05 μg L^{-1} (or 50 ng L^{-1}).[4] The emerging environmental issue relating to antibiotic residues not only threatens public health but also compromises the effectiveness of the drugs themselves (i.e., contributing to antibiotic resistance). Among the quinolone antibiotics class, ciprofloxacin (CFX) is widely utilized due to its broad-spectrum activity against many pathogenic bacteria. After medication, CFX can be partially broken down by metabolism in human or animal bodies and largely excreted in its pharmacologically active forms.[5–6] Therefore, practical and economical processes are urgently required to reduce the CFX antibiotic discharge into the environment.

To overcome this environmental challenge, various processes have been applied to degrade or remove contaminants, including adsorption, photocatalysis, biodegradation, electrochemical treatment.[7] While conventional treatments like filtration and coagulation/ flocculation/ sedimentation require subsequent treatments to treat the pollutants, other current techniques such as membrane, ozonation and Fenton process often bring weakness in the high costs of installation, investment and operation.[1, 8, 9] Consequently, photocatalytic semiconductors based on the advanced oxidation process (AOPs) are highly recommended This technology is recognized largely as one of the most low-cost, sustainable, and environmentally friendly approaches for wastewater treatment.[10–13]

Monoclinic bismuth orthovanadate ($BiVO_4$), an *n*-type semiconductor, widely recognized as a promising solar-driven photocatalyst due to its narrow band gap (2.4 eV). $BiVO_4$ exhibits outstanding features: nontoxic nature, high stability towards photocorrosion, low production cost, relatively strong oxidation properties for the decomposition of organic pollutants, and its promising application as a photoanode material for water splitting. Nevertheless, the performance of the single component $BiVO_4$ is still restricted by the fast recombination of photoinduced carriers (electron/hole pairs).[14–17] To date, various alternative strategies have been investigated to overcome limitation of $BiVO_4$, including cocatalyst loading, construction of heterostructures, and substitution of the metal cation or anion.[18–22] For the research approach of constructing heterostructures, $BiVO_4$ was assembled with another semiconductor to form a heterojunction that can significantly reduce the combination and speed up the separation rate of photogenerated charge carriers.[23–25] To couple with $BiVO_4$ to form these heterostructures, one of the most frequently-used semiconductors that serve as a second component is anatase titanium dioxide (TiO_2) – a well-known photocatalyst with the band gap value of 3.2 eV to benefit its high chemical stability, excellent photocatalytic activity.[26–30] Although numerous researches on TiO_2/$BiVO_4$ photocatalytic composites have been reported, an optimized synthesis procedure

has not been established. In addition, most published synthesis procedures of these photocatalytic composites usually involve multi-steps, and to date, only limited number of one-pot approaches have been described in literature.[28,30] Y.-R. Lv *et al*. applied one-pot hydrothermal procedure to synthesize $TiO_2/BiVO_4$ nanocomposites with Bi^{3+}:Ti^{4+} molar ratios less than 0.2:1.[28] The photocatalytic efficiency of 60 % for photodegradation reaction of Rhodamine B over the optimized sample after 4 hours of visible-light irradiation. For $TiO_2/BiVO_4$ system, to the best of our knowledge, TiO_2-rich composites were studied the most,[19,26–28,30] while only one work focusing on $BiVO_4$-rich composites with Bi^{3+}:Ti^{4+} molar ratio equals to or over 1:1 was reported.[29] However, the effects of Bi^{3+}:Ti^{4+} molar ratio on the photocatalytic efficiency of $BiVO_4$-rich composites were not studied systematically by K. T. Drisya *et al* with only investigated Bi^{3+}:Ti^{4+} molar ratio value of 1:0.6. This might originate from the fact these researches focused mainly on improving Vis-photocatalytic performances of TiO_2 via designing TiO_2-based composites, in which $BiVO_4$ played as role as a dopant or a minor component, rather than hindering the fast recombination of photoinduced electron-hole pairs, the main drawback of the pure $BiVO_4$, via designing $BiVO_4$-rich composites. In other words, the design of a heterogeneous junction to enhance photo-induced charge separation, and consequently improve the photocatalytic performance of $BiVO_4$-rich composites containing anatase as a minor component for photodegradation of antibiotics in general, and ciprofloxacin in particular, has not been mentioned yet.

Hence, this research aimed to synthesize $TiO_2/BiVO_4$ semiconductors with Bi^{3+}:Ti^{4+} molar ratio equals to or greater than 1:1 using hydrothermal method in a basic medium, and their photocatalytic activities were determined by the degradation of ciprofloxacin antibiotic in aqueous solution under visible-light irradiation.

EXPERIMENTAL

Synthesis of photocatalysts

All the reagents were of analytical grade and used without any further purification. Typically, 1 mmol $Bi(NO_3)_3.5H_2O$ (Acros) and a certain amount of TiO_2 (Sigma-Aldrich) were dissolved in 2 mL of 4 M HNO_3 solution, while 1 mmol NH_4VO_3 (Sigma-Aldrich) was dissolved in 10 mL double distilled water at 80 ºC. The two solutions were mixed and transferred into a 120-mL Teflon-lined stainless-steel autoclave. The pH of these mixtures was adjusted to 11 by addition of 12 mL of concentrated NH_3 solution (25 %). Subsequently, the autoclave was filled with double distilled water up to 75 % of its capacity. The sealed autoclave was heated at 180 ºC for 24 hours under autogenous pressure. After undergoing hydrothermal treatment, the precipitated solids were collected and washed with double distilled water until reaching a neutral medium. Finally, the yellow precipitates were obtained after drying naturally in air.

For the synthesis of the pure $BiVO_4$, the same synthesis procedure was performed except that no TiO_2 was added. The three composite products were denoted as $1TiO_2/4BiVO_4$,

$1TiO_2/2BiVO_4$ and $1TiO_2/1BiVO_4$ corresponding to the sample with the Bi^{3+}:Ti^{4+} molar ratios of 4:1, 2:1 and 1:1, respectively.

Characterization methods

The crystalline phases of the as-synthesized samples were determined by using an X-ray diffractometer (XRD, D8 ADVANCE, Bruker). The synthesized samples were also characterized by field-emission scanning electron microscopy (FESEM, Hitachi S-4800), high resolution transmission electron microscopy (HR-TEM, Jeol 2100), and diffuse-reflectance UV-Vis spectrometry (DR-UV-Vis, Jasco V670).

Photocatalytic properties

The photocatalytic activities of the studied composites were estimated by the degradation of ciprofloxacin solution (0.5 ppm) at room temperature under visible-light irradiation. Typically, 0.025 g photocatalyst was added to 100 mL the antibiotic solution in each experiment. The solution was stirred for one hour in dark for reaching of adsorption-desorption equilibrium. The suspension was then irradiated by a visible-light source provided by a 100 W halogen lamp with the center wavelength of 700 nm from a distance of 20 cm. At certain interval times (30, 60, 90 and 120 min) during irradiation, 5 mL of the tested solution was taken out and was then filtrated with 0.22 µm membrane prior to concentration determination by using a LC-MS/MS system (ACQUITY UPLC H-class/ Xevo-TQ, USA).

The photocatalytic degradation efficiency was calculated by the following equation:

$$H\% = \frac{Co - Ct}{Co} \times 100\% \quad (1)$$

Wherein: C_o is the initial concentration of ciprofloxacin (without any photocatalyst);

C_t is the remaining concentration of ciprofloxacin in the solution at time t / min after irradiation.

RESULTS AND DISCUSSION

Crystalline structure

From XRD diagrams (Fig. 1), it can be confirmed that the monoclinic scheelite structure of $BiVO_4$ (*ms*-$BiVO_4$) was successfully synthesized for all studied samples, namely, pure $BiVO_4$, $1TiO_2/4BiVO_4$, $1TiO_2/2BiVO_4$ and $1TiO_2/1BiVO_4$. Particularly, diffraction peaks at 2-theta values of 18.65; 18.98; 28.94; 30.54; 34.49; 35.22; 39.78 ° are corresponding to (1 1 0); (0 1 1); (-1 3 0); (0 4 0); (2 0 0); (0 0 2); (2 1 1) lattice planes of monoclinic scheelite structure of $BiVO_4$ (JCPDS card No. 14-0688), respectively. Moreover, the doublet peaks at 2-theta values of around 18.5 and 35 ° can be a useful mark to distinguish a monoclinic scheelite phase and a tetragonal scheelite phase of $BiVO_4$.[31]

The result indicated that, by carrying out the hydrothermal synthesis procedure in basic medium, the monoclinic scheelite structure was controlled to grow as a unique crystalline phase of $BiVO_4$ and the coexistence of monoclinic scheelite and tetragonal zircon as reported previously was avoided.[32] In another word, the formation of tetragonal zircon phase, a thermodynamically stable polymorph of $BiVO_4$ under the acidic medium of hydrothermal synthesis reaction, was totally inhibited.

In addition, for all XRD patterns of $TiO_2/BiVO_4$ composite samples, a set of diffraction peaks at 2-theta values of 25.6; 38.3; 48.8 ° were detected, indicating the existence of anatase TiO_2 (JCPDS card No. 21-1272).[33] Furthermore, no other impurity was found in all investigated samples, similar to those published for $TiO_2/BiVO_4$ composites.[28-30] The intensity of anatase TiO_2 increased monotonously as desirable with the TiO_2 content in the composite samples when the Bi^{3+}:Ti^{4+} molar ratio decreased from 4:1 to 1:1. It is also worthy to note that by the coupling with anatase TiO_2 to form photocatalytic composites, the calculated lattice parameters of the monoclinic scheelite $BiVO_4$ existed in pure $BiVO_4$, $1TiO_2/4BiVO_4$, $1TiO_2/2BiVO_4$ and $1TiO_2/1BiVO_4$ samples were almost unchanged as tabulated in Table 1.

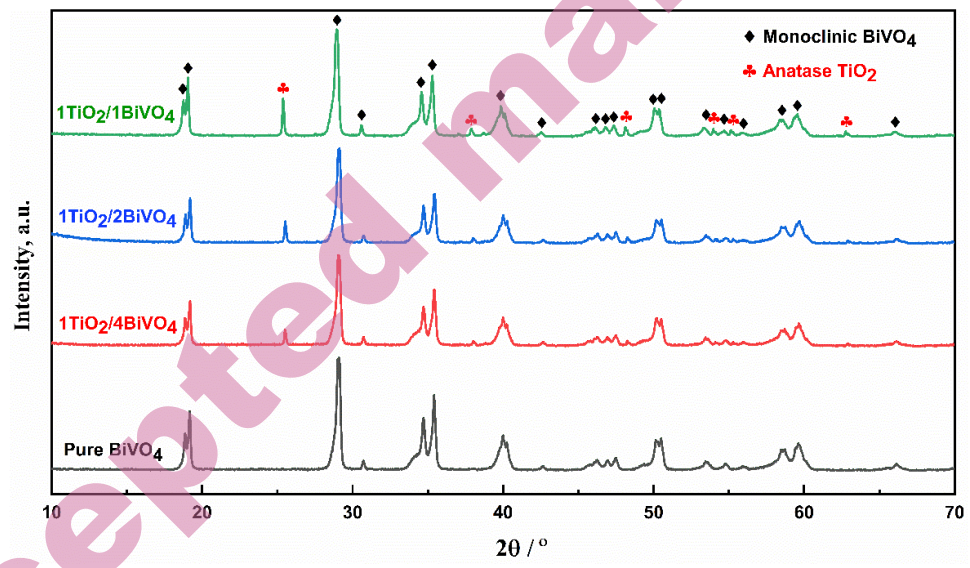

Fig. 1. XRD patterns of pure $BiVO_4$ and $TiO_2/BiVO_4$ composite samples

Table 1: The calculated lattice parameters of pure $BiVO_4$, $1TiO_2/4BiVO_4$, $1TiO_2/2BiVO_4$ and $1TiO_2/1BiVO_4$ samples

Sample	Lattice parameters			
	a (Å)	b (Å)	c (Å)	β (°)
Pure $BiVO_4$	5.194(2)	11.699(2)	c = 5.090(1)	90.38(1)
$1TiO_2/1BiVO_4$	5.195(1)	11.701(3)	c = 5.089(2)	90.37(2)
$1TiO_2/2BiVO_4$	5.194(3)	11.700(2)	c = 5.091(3)	90.38(2)
$1TiO_2/4BiVO_4$	5.194(1)	11.700(1)	c = 5.092(2)	90.38(1)

Microstructures

To investigate the morphology of the synthesized $TiO_2/BiVO_4$ composite, the $1TiO_2/4BiVO_4$ and $1TiO_2/1BiVO_4$ samples were subjected to SEM observation as

examples. From the SEM image of the composite material as shown in Figs. 2 and 3, it reveals the presence of spherical-like TiO_2 nanoparticles with the average grain size of 120 nm embedded on the surface of $BiVO_4$ when compared to that of the pure $BiVO_4$. This agrees well with the statement given for XRD patterns. For both cases of pure $BiVO_4$ and $TiO_2/BiVO_4$ composites, the $BiVO_4$ nanoplates with average width of 200 nm and length of 300 nm are observed.

Compared to the case of commercialized TiO_2 precursor, the shape and average grain size TiO_2 nanoparticles existed in $TiO_2/BiVO_4$ composite are almost unchanged, suggesting the inhibition role of basic medium on grain growth of titanium dioxide, TiO_2 (Fig. 3).[34]

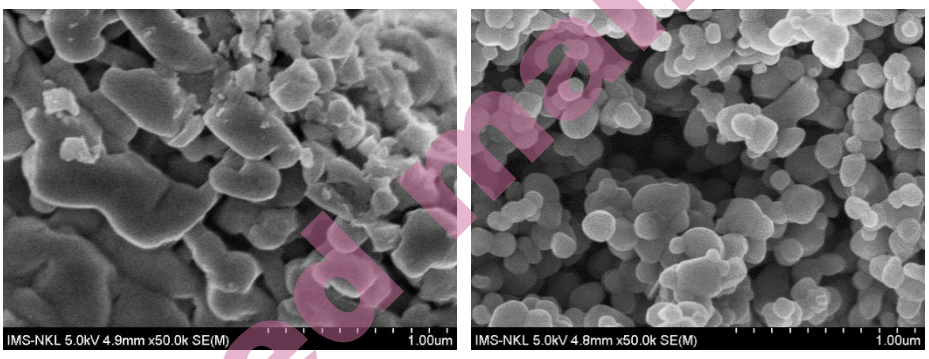

(a) (b)

Fig. 2. SEM images of a) pure $BiVO_4$ and $1TiO_2/4BiVO_4$ samples

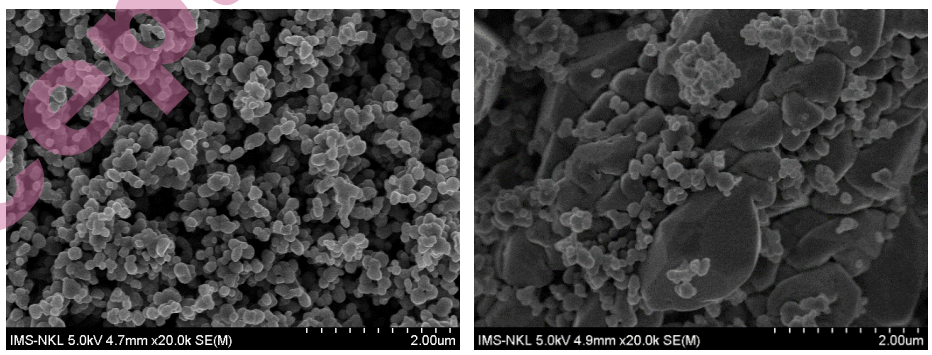

(a) (b)

Fig. 3. SEM images of a) commercialized TiO_2 precursor and b) $1TiO_2/1BiVO_4$ composite.

To investigate further the microstructure of as-synthesized samples, the HR-TEM image and its corresponding FFT pattern of $1TiO_2/1BiVO_4$ composite sample were presented in Figs. 4a and 4b, respectively. Two lattice fringe spacings of 0.292 and 0.467 nm with an interfacial angle of 66.5° that be assigned to (0 4 0)

and (0 1 1) lattice planes of *m*s-$BiVO_4$, respectively, were observed in both HR-TEM image and its corresponding FFT pattern. At the same time, two other lattice fringe spacings of 0.347 and 0.469 nm that formed an included angle of 68.3° were interpreted respectively as (0 1 1) and (0 0 2) lattice planes of anatase TiO_2 phase. These calculated results indicated obviously that the investigated $1TiO_2/1BiVO_4$ contained both *m*s-$BiVO_4$ and anatase TiO_2 particles. Moreover, as shown in Fig. 4a, the direct contact between *m*s-$BiVO_4$ nanoplates and anatase TiO_2 nanoparticles was observed, suggesting the formation of heterojunction between them.

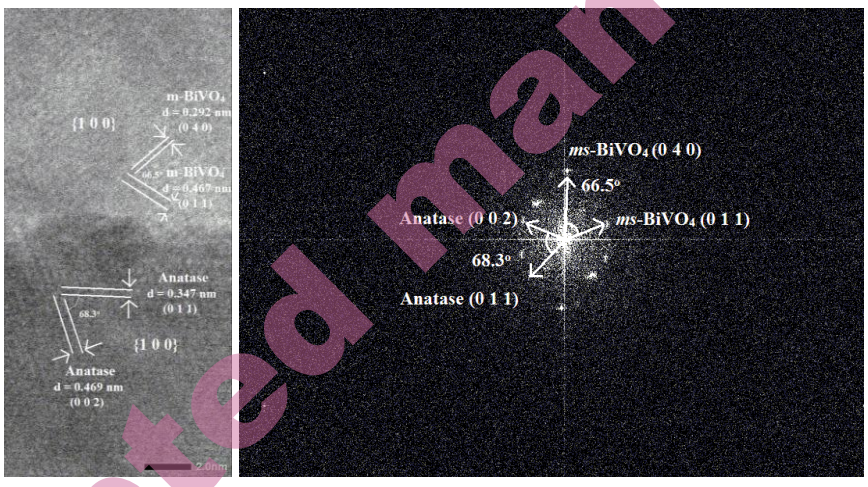

(a) (b)

Fig. 4: a) HR-TEM image and b) its corresponding FFT pattern of $1TiO_2/1BiVO_4$ composite sample

Diffuse-reflectance UV-Vis spectra

From the spectra received by DR UV-Vis measurements as shown in Fig. 5, a derived Tauc's plot was then depicted in Fig. 6 that showed the relationship between hν (the energy of the light) and $(\alpha h\nu)^2$, where α was the absorption coefficient of the material. Based on extrapolating the linear region in Fig. 6, the band gap (E_g) values of synthesized photocatalysts were estimated to be 2.43, 2.42 and 2.44 eV, corresponding to the 4:1, 2:1 and 1:1 composite samples, respectively. The results showed the absorption feature of the composite materials and the pure $BiVO_4$ as well (E_g = 2.42 eV) in visible region did not have a significant difference. Therefore, to conclude which was as-prepared material exhibiting the best photocatalytic activity, it is necessary to perform further photocatalytic tests with the analyte (i.e., ciprofloxacin). However, the band gap

values of around 2.4 eV suggested photocatalytic experiments should be performed under visible-light irradiation.

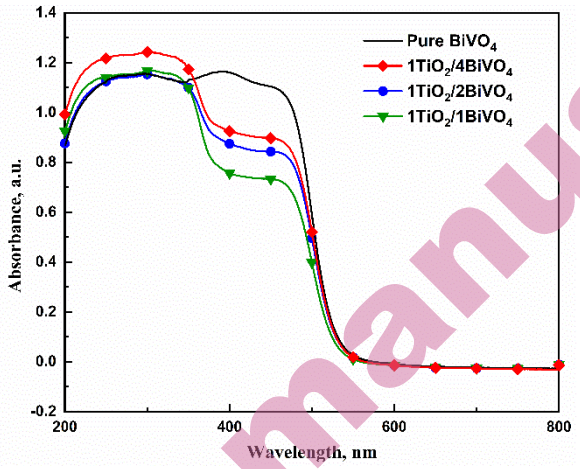

Fig. 5. Diffuse-reflectance UV-Vis spectra of pure $BiVO_4$ and $BiVO_4/TiO_2$ composites

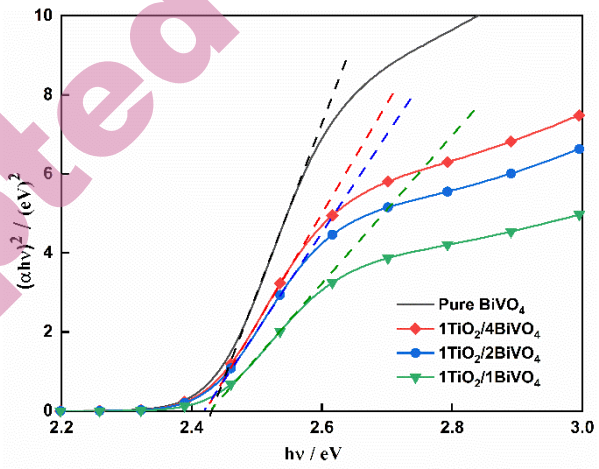

Fig. 6. Tauc's plots of pure $BiVO_4$ and $BiVO_4/TiO_2$ composites

Photocatalytic activities

Photocatalytic activities of as-synthesized samples were evaluated according to the degradation of ciprofloxacin. These experiments included the photocatalytic degradation of only ciprofloxacin solution without any photocatalyst; ciprofloxacin and pure $BiVO_4$ (CFX+$BiVO_4$); ciprofloxacin and 4:1 composite (CFX+1TiO_2/4$BiVO_4$); and ciprofloxacin and 1:1 composite (CFX+1TiO_2/1$BiVO_4$). The photocatalytic degradation efficiency after that was illustrated in Fig. 7.

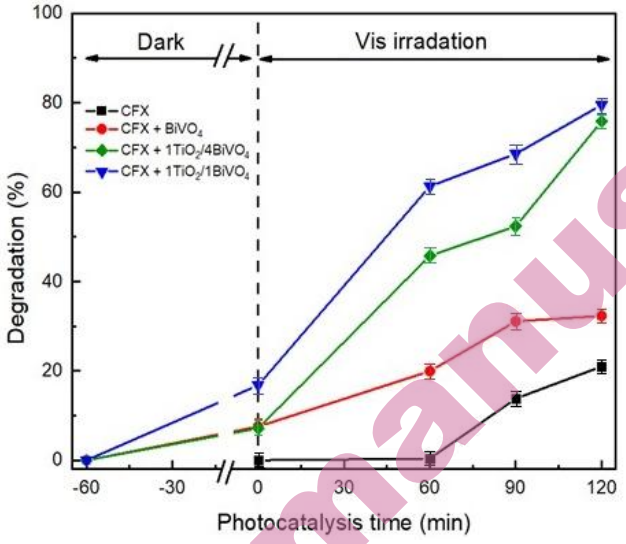

Fig. 7. Photocatalytic degradation efficiency of ciprofloxacin with and without the as-prepared photocatalysts under irradiation using a 100 W halogen lamp

The results showed that after 120 minutes under visible-light irradiation, while ciprofloxacin was degraded only 32 % in the activity of pure $BiVO_4$, it was removed 75 and 80 % by $1TiO_2/4BiVO_4$ and $1TiO_2/1BiVO_4$, respectively. Thus, similar to the case of previous works, the composite materials were visible-light photoactive with their photodegradation efficiency was obviously twice as high as that of the pure $BiVO_4$ sample.[19,23,28] The existence of a heterojunction formed between $BiVO_4$ nanoplates and embedded 120-nm spherical-like TiO_2 nanoparticles was probably attributed to this significant improvement in ciprofloxacin photodegradation efficiency of the studied $TiO_2/BiVO_4$ composites with respect to that of the pure $BiVO_4$. Also, it can be derived from Fig. 7 that, after reaching of adsorption-desorption equilibrium, the CFX adsorption percentage of pure $BiVO_4$ and $1TiO_2/4BiVO_4$ samples was around 7 % and was almost the same while that of $1TiO_2/1BiVO_4$ sample was higher (17 %). That can be explained by the fact that, the $1TiO_2/1BiVO_4$ sample possessed the higher amount of spherical-like anatase TiO_2 nanoparticles with relatively high specific surface area (of around 10 m^2/g) than pure $BiVO_4$ and $1TiO_2/4BiVO_4$ samples. In addition, the kinetics of the CFX photodegradation reactions over pure $BiVO_4$ and $1TiO_2/1BiVO_4$ samples was also investigated. The obtained results indicated that the CFX photodegradation reactions over these two samples can be described by the first-order kinetic equation (Fig. 8):

$$\ln(C_0/C_t) = kt \quad (2)$$

where C_0 is the initial CFX concentration, C_t is the CFX concentration at reaction time t, and k is the observed first-order rate constant. The photodegradation reaction rate constant of 0.00899 min^{-1} calculated for the $1TiO_2/1BiVO_4$ sample was about 3.8 times higher than that of the pure $BiVO_4$ sample (0.00235 min^{-1}) (Fig. 8, the inset).

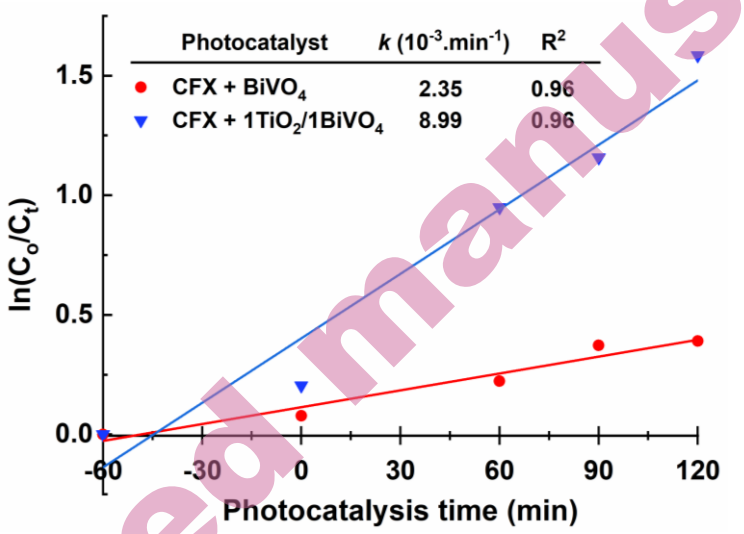

Fig. 8. The dependence of $ln(C_0/C_t)$ on the visible-light irradiation time of the optimized $1TiO_2/1BiVO_4$ and the pure $BiVO_4$ samples.

From m/z values obtained from LC-QTOFMS spectrum for the photodegradation of ciprofloxacin over the optimized $1TiO_2/1BiVO_4$ sample under visible-light irradiation, two major possible intermediate products denoted as CFX1 and CFX2 were detected (Table 2). The ion at m/z = 314.1 can be assigned to the dehydration of the CFX to produce CFX1.[35] The quinolone moiety of the CFX was attacked by the produced •OH radicals, leading to a decarboxylation process to form CFX2 with m/z value of 288.1.[36] Based on these data, a CFX photocatalytic degradation pathways under visible-light irradiation was proposed as shown in Fig. 8.[36,37] Accordingly, as a first step of the photodegradation reaction, CFX2 was formed as an intermediate product from the CFX under visible-light irradiation. By increasing the photocatalytic reaction time further, CFX2 will be degraded into smaller substances. The photocatalytic reaction will complete when all available intermediate products of photodegradation reaction were mineralized into H_2O and CO_2 as final compounds.[36,37]

Table 2: Major m/z values and chemical formula of possible intermediate products detected by LC-MS/MS for the photodegradation of ciprofloxacin under visible-light irradiation

No.	Intermediate products	m/z	Possible chemical formula
1	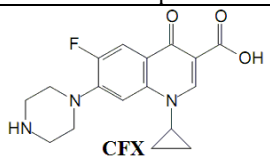 CFX	332.1	$C_{17}H_{18}FN_3O_3$
2	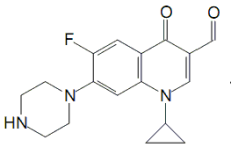 CFX1	314.1	$C_{17}H_{17}FN_3O_2$
3	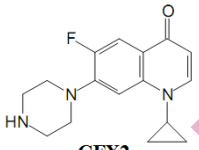 CFX2	288.1	$C_{16}H_{18}FN_3O$

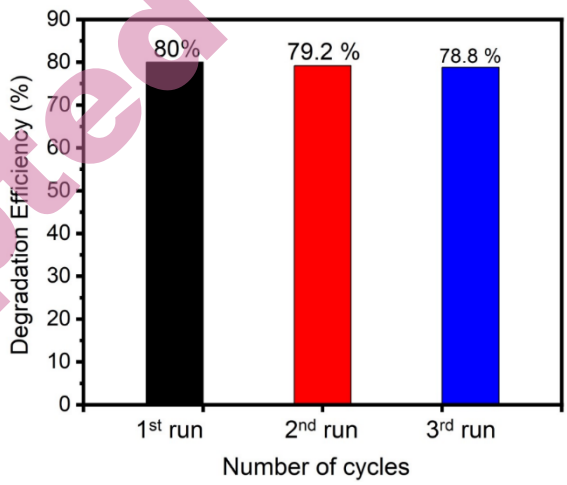

Fig. 9. Photodegradation recyclability test of ciprofloxacin over the optimized $1TiO_2/1BiVO_4$ sample under visible-light irradiation.

As shown in Fig. 9 were the recyclability testing results of CFX over the optimized $1TiO_2/1BiVO_4$ sample for three recycling photocatalytic runs under visible-light irradiation. The results showed that the photodegradation efficiency decreased slightly to 79.2 and 78.8% for the second and third cycles from the value of 80 % for the first cycle, respectively. The CFX photodegraded species existing on the composite's surface might block the photoactive sites, leading to this slight

decrease in photodegradation efficiency. This implied that our optimized $TiO_2/BiVO_4$ composite sample can be reusable with high photocatalytic stability.

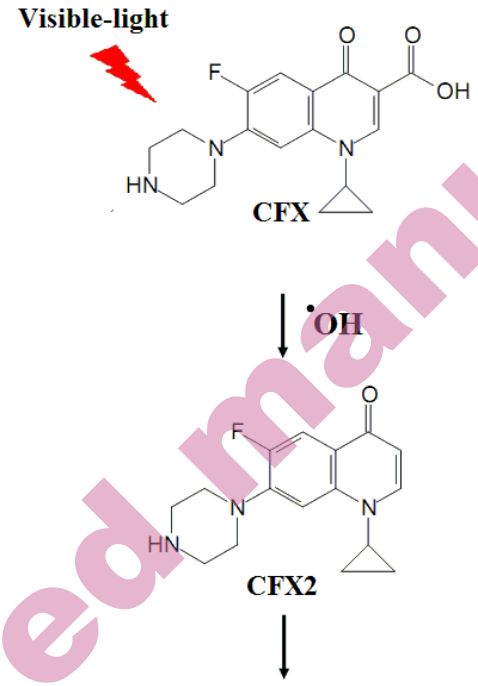

Scheme 1. Proposed reaction pathways and intermediate products generated in the photodegradation reaction of ciprofloxacin under visible-light irradiation

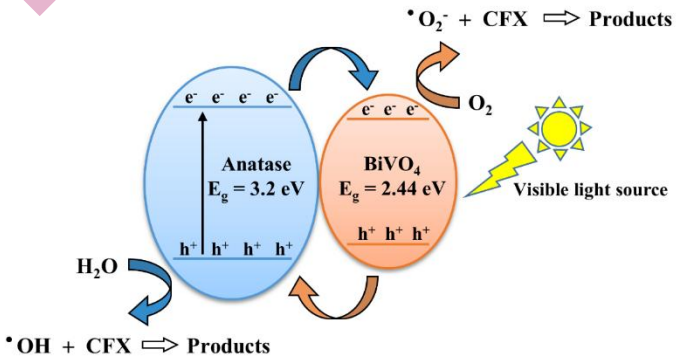

Scheme 2. The proposed photocatalytic mechanism of $1TiO_2/1BiVO_4$ sample for CFX photodegradation under visible-light irradiation.

Similar to previously published results,[27,38,39] the photocatalytic activity-enhancing mechanism for CFX photodegradation in aqueous medium under visible-light irradiation over the $BiVO_4$-rich composites containing anatase as a minor component can be proposed as follows:

1) The incident light was absorbed mainly by the Vis-photoactive $BiVO_4$ component of $TiO_2/BiVO_4$ composite, leading to the generation of photo-induced pairs electron-hole pairs.:

$$h\upsilon + ms\text{–}BiVO_4 \rightarrow h^+_{VB} + e^-_{CB} \quad (3)$$

2) Via the heterojunction formed between *ms*-$BiVO_4$ nanoplates and TiO_2 nanoparticles, the photo-induced electrons in the conduction band of anatase TiO_2 were transferred to that of $BiVO_4$ while holes in the valence band of $BiVO_4$ were transferred to that of anatase TiO_2 under visible-light irradiation (Scheme 2).

3) The photo-induced charge transfer via heterojunction led to the increase in lifetime of electron-charge separation of the $TiO_2/BiVO_4$ composites. This transfer was supposed to depend on the Bi^{3+}:Ti^{4+} molar ratio of this photocatalytic composite. The highest photocatalytic efficiency was found for the composite with the highest Bi^{3+}:Ti^{4+} molar ratio of 4:1 while the pure BiVO4 sample exhibited the fastest photo-induced charge recombination due to the absence of a charge transferring process. The further increase in TiO_2 to decrease Bi^{3+}:Ti^{4+} molar ratio down to 1:1, however, lowered the composite's photocatalytic activity. This was probably due to multiple trapping of photo-induced charges.[35]

4) At the composite's surface, the dissolved oxygen in aqueous medium was oxidized by photo-induced electrons to active free radical species such as $O_2^{\cdot-}$, $OH^{\cdot}$:

$$e^- + O_2 \rightarrow O_2^{\cdot-} \quad (4)$$

$$O_2^{\cdot-} + H^+ + e^- \rightarrow OH^{\cdot} + OH^- \quad (5)$$

5) The electron donors (H_2O) reacted with photo-induced holes at the composite's surface to produce $OH^{\cdot}$:

$$h^+ + H_2O \rightarrow OH^{\cdot} + H^+ \quad (6)$$

6) The photo-induced holes and other freshly-produced free radicals like $O_2^{\cdot-}$, $OH^{\cdot}$, etc. oxidized the surface-adsorbed CFX (CFX_{ad}) molecules to form photodegraded species like CO_2, H_2O and other by-products:

$$CFX_{ad} + h^+ / OH^{\cdot} / O_2^{\cdot-} \rightarrow CO_2 + H_2O + \text{other by–products} \quad (7)$$

CONCLUSION

Pure $BiVO_4$ and three $TiO_2/BiVO_4$ composite samples with molar ratios of 1:1, 2:1 and 4:1 were readily synthesized at a pH of 11 via hydrothermal method. Under the hydrothermal conditions, only a single-phase scheelite monoclinic polymorphic type of $BiVO_4$ (*ms*- $BiVO_4$) was obtained, and the $BiVO_4$ nanoplates had average to and width of 200 nm and length of 300 nm.

Compared to the case of the pure $BiVO_4$, the photocatalytic degradation rate of ciprofloxacin over the $TiO_2/BiVO_4$ composites was significantly higher, and the $1TiO_2/1BiVO_4$ sample was expected to be the most potential photocatalyst with its highest efficiency of ciprofloxacin degradation after 120 minutes under visible-light irradiation. The enhancement in ciprofloxacin removal of the studied $TiO_2/BiVO_4$ composites might have originated from the existence of a heterojunction formed between $BiVO_4$ nanoplates and embedded 120-nm spherical-like TiO_2 nanoparticles.

Acknowledgements: We thank the "Program on development of Basic science s in the field of Chemistry, Life Science and Marine Science during 2017-2025" issued by Vietnames government for providing research fund under the project coded ĐTĐL.CN-47/21.

И З В О Д

СИНТЕЗА $TiO_2/BiVO_4$ КОМПОЗИТА ФОТОАКТИВНОГ НА ВИДЉИВУ СВЕТЛОСТ ЗА ФОТОКАТАЛИТИЧКУ ДЕГРАДАЦИЈУ ЦИПРОФЛОКСАЦИНА

THU LOAN DANG[1], VU VAN TU[2], THI HUE NGUYEN[2], DUC VAN NGUYEN[3], AND THI THAO TA[1]

[1]Faculty of Chemistry, VNU University of Science, 19 Le Thanh Tong, 100000, Vietnam, [2]Institute of Science and Technology for Energy and Environment, Vietnam Academy of Science and Technology, 18 Hoang Quoc Viet, Nghia Do Ward, Hanoi 100000, Vietnam, and [3]Institute of Materials Science, Vietnam Academy of Science and Technology, 18 Hoang Quoc Viet, Nghia Do Ward, Hanoi 100000, Vietnam.

Чист $BiVO_4$ и три $TiO_2/BiVO_4$ композитна фотокатализатора са моларним односима Bi^{3+}: Ti^{4+} од 1:1, 2:1 и 4:1 успешно су синтетисани по први пут применом „one-pot" хидротермалне процедуре за фотодеградацију ципрофлоксацина. Извођење хидротермалне реакције у базној средини резултирало је стварањем једнофазног моноклиничног $BiVO_4$ (ms-$BiVO_4$) структуре шелита у узорцима композита. Микроструктурна анализа показала је сферичне наночестице TiO_2, просечне величине зрна од 120 nm, које су уграђене на површину наноплоча $BiVO_4$. Оптимизовани композит показао је константу брзине реакције фотодеградације ципрофлоксацина која је била око 3.8 пута већа у поређењу са узорком чистог $BiVO_4$. Ово значајно побољшање приписује се формирању $TiO_2/BiVO_4$ хетеројединења, који поспешује ефикасно раздвајање наелектрисања. Ово истраживање проширује знање о дизајнирању композита богатих са $BiVO_4$ (са моларним односом Bi^{3+}:Ti^{4+} ≥ 1:1) путем инжењеринга хетерогених спојева ради побољшања фотокаталитичке активности изнад нивоа чистог $BiVO_4$. Ово истраживање је такође пружило перспективу о коришћењу композита богатих $BiVO_4$ као ефикасних фотокатализатора за деградацију антибиотика у воденим растворима под зрачењем видљивом светлошћу.

(Примљено 13. јуна; ревидирано 30. јуна; прихваћено 2. децембра 2026.)

REFERENCES

1. V. Homem, L. Santos, *J. Environ. Manage.* **92** (2011) 2304 (https://doi.org/10.1016/j.jenvman.2011.05.023)

2. C. Yan, Y. Yang, J. Zhou, M. Liu, M. Nie, H. Shi, L. Gu, *Environ. Pollut.* **175** (2013) 22 (https://doi.org/10.1016/j.envpol.2012.12.008)
3. C. S. Lundborg, A. Tamhankar, *BMJ.* **358** (2017) j2440 (https://doi.org/10.1136/bmj.j2440)
4. Organization, W.H., *Pharmaceuticals in drinking-water,* World Health Organization, Geneva, 2012, 35p. (https://apps.who.int/iris/handle/10665/44630)
5. S. Babić, M. Periša, I. Škorić, *Chemosphere*. **91** (2013) 1635 (https://doi.org/10.1016/j.chemosphere.2012.12.072)
6. J. Porras, C. Badoya, J. Silva-Agredo, A. Santamaría, J. J. Fernández, R. A. Torres-Palma, *Water Res.* **94** (2016) 1 (https://doi.org/10.1016/j.watres.2016.02.024)
7. Z. Wei, J. Liu, W. Shangguan, *Chinese J. Catal.* **41** (2020) 1440 (https://doi.org/10.1016/S1872-2067(19)63448-0)
8. K. Košutić, D. Dolar, D. Ašperger, B. Kunst, *Sep. Purif.* **53** (2007) 244 (https://doi.org/10.1016/j.seppur.2006.07.015)
9. C. A. Igwegbe, S. N. Oba, C. O. Aniagor, A. G. Adeniyi, *Ind. Eng. Chem. Res.* **93** (2021) 57 (https://doi.org/10.1016/j.jiec.2020.09.023)
10. M. N. Chong, B. Jin, C. W. K. Chow, C. Saint, *Water Res.* **44** (2010) 2997 (https://doi.org/10.1016/j.watres.2010.02.039)
11. S. Dong, J. Feng, M. Fan, Y. Pi, L. Hu, X. Han, M. Liu, J. Sun, J. Sun, *RSC Adv.* **5** (2015) 14610 (https://doi.org/10.1039/C4RA13734E)
12. W. S. Koe, J. W. Lee, W. C. Chong, Y. L. Pang, L. C. Sim, *Environ. Sci. Pollut.* **27** (2020) 2522 (https://doi.org/10.1007/s11356-019-07193-5)
13. S. Zhu, D. Wang, *Adv. Energy Mater.* **7** (2017) 1700841 (https://doi.org/10.1002/aenm.201700841)
14. A. Malathi, J. Madhavan, M. Ashokkumar, P. Arunachalam, *Appl. Catal. A: Gen.* **555** (2018) 47 (https://doi.org/10.1016/j.apcata.2018.02.010)
15. M. Guo, Q. He, A. Wang, W. Wang, Z. Fu, *Cryst.* **6** (2016) 81 (https://doi.org/10.3390/cryst6070081)
16. O. Monfort, G. Plesch, *Environ. Sci. Pollut.* **25** (2018) 19362 (https://doi.org/10.1007/s11356-018-2437-9)
17. H. L. Tan, R. Amal, Y. H. Ng, *J. Mater. Chem. A* **5** (2017) 16498 (https://doi.org/10.1039/C7TA04441K)
18. Y. Li, D. Liao, T. Li, W. Zhong, X. Wang, X. Hong, H. Yu, J. *Colloid Interface Sci.* **570** (2020) 232 (https://doi.org/10.1016/j.jcis.2020.02.093)
19. S. Obregón, G. Colón, *RSC Adv.* **4** (2014) 6920 (https://doi.org/10.1039/c3ra46603e)
20. X.-J. Wen C. G. Niu, L. Zhang, C. Liang, H. Guo, G. M. Zeng, *J. Catal.* **358** (2018) 141 (https://doi.org/10.1016/j.jcat.2017.11.029)
21. B. Zhang, H. Zhang, Z. Wang, X. Zhang, X. Qin, Y. Dai, Y. Liu, P. Wang, Y. Li, B. Huang, *Appl. Catal.* **211** (2017) 258 (https://doi.org/10.1016/j.apcatb.2017.03.078)
22. D. B. Hernández-Uresti, C. Alanis-Moreno, D. Sanchez-Martinez, *Mater. Sci. Semicond.* **102** (2019) 104585 (https://doi.org/10.1016/j.mssp.2019.104585)
23. K. Pingmuang, J. Chen, W. Kangwansupamonkon, G. G. Wallace, Sukon Phanichphant, A. Nattestad, *Sci. Rep*., **7** (2017) 8929 (https://doi.org/10.1038/s41598-017-09514-5)
24. Z. Ye, X. Xiao, J. Chen, Y. Wang, *Photochem. Photobiol. A: Chem*., **368** (2018) 153 (https://doi.org/10.1016/j.jphotochem.2018.09.044).

25. J. Yang, Q. Shi, R. Zhang, M. Xie, X. Jiang, F. Wang, X. Cheng, W. Han, *Carbon*, **138** (2018) 118 (https://doi.org/10.1016/j.carbon.2018.06.003)
26. Y. Hu, W. Chen, J. Fu, M. Ba, F. Sun, P. Zhang, J. Zou, *App. Surf. Sci.*, **436** (2018) 319 (https://doi.org/10.1016/j.apsusc.2017.12.054)
27. W. Li, Z. Wang, D. Kong, D. Du, M. Zhou, Y. Du, T. Yan, J. You, D. Kong, *J. Alloys Compd*., **688** (2016) 703 (http://dx.doi.org/10.1016/j.jallcom.2016.07.249)
28. Y.-R. Lv, C.-J. Liu, R.-K. He, X. Li, Y.-H. Xu, *Mater. Res. Bull*., **117** (2019) 35 (https://doi.org/10.1016/j.materresbull.2019.04.032)
29. K. T. Drisya, M. Solís-López, J. J. Ríos-Ramírez, J. C. Durán-Álvarez, A. Rousseau, S. Velumani, R. Asomoza, A. Kassiba, A. Jantrania, H. Castaneda, *Sci. Rep*. **10** (2020) 13507 (https://doi.org/10.1038/s41598-020-69032-9)
30. G, Longo, F. Fresno, S. Gross, U. L. Štangar, *Environ. Sci. Pollut. Res.* **21** (2014) 11189 (https://doi.org/10.1007/s11356-014-2624-2)
31. S. Okunaka, H. Tokudome, Y. Hitomi, R. Abe, *J. Mater. Chem. A* **4** (2016) 3926 (https://doi.org/10.1039/C5TA09789D)
32. Y. Zhou, G. Jiang, R. Wang, X. Wang, R. Hu, X. Xi, *J. Fiber Bioeng. Inform.* **5** (2012) 181 (https://doi.org/10.3993/jfbi06201207)
33. L. Zhang, G. Tan, S. Wei, H. Ren, A. Xia, Y. Luo, *Ceram. Int.* **39** (2013) 8597 (https://doi.org/10.1016/j.ceramint.2013.03.106)
34. D. Li, H. Song, X. Meng, T. Shen, J. Sun, W. Han, X. Wang, *Nanomater. (Basel, Switzerland)* **10** (2020) 546 (https://doi.org/10.3390/nano10030546).
35. M. Jiméenez-Salcedo, M. Monge, M. T. Tena, *Chemosphere* **247** (2020) 125910 (https://doi.org/10.1016/j.chemosphere.2020.125910)
36. T. Ahamad, M. Naushad, S. M. Alshehri, *Chem. Eng. J*. **417**, (2021) 127969 (https://doi.org/10.1016/j.cej.2020.127969)
37. T. G. Vasconcelos, D. M. Henriques, A. König, A. F. Martins, K. Kümmerer, *Chemosphere* **76** (2009) 487–493 (https://doi.org/10.1016/j.chemosphere.2009.03.022)
38. Y. Kang, Y. Yang, L.-C. Yin, X. Kang, G. Liu, H.-M. Cheng, *Adv. Mater.* **27** (2015) 4572 (https://doi.org/10.1002/adma.201501939)
39. Nguyen Duc Van, Do Thi Anh Thu, Ngo Thi Hong Le, Doan Tuan Anh, *Mater. Sci. Eng. B* **278** (2022) 115616 (https://doi.org/10.1016/j.mseb.2022.115616)